Improved Model of Hydrated Calcium Ion for Molecular Dynamics Simulations Using Classical Biomolecular Force Fields

Jejoong Yoo,[1,2] James Wilson,[1] Aleksei Aksimentiev,[1,2,3]

[1] *Department of Physics, University of Illinois at Urbana–Champaign, 1110 West Green Street, Urbana, IL 61801*

[2] *Center for the Physics of Living Cells, Urbana, IL 61801*

[3] *Beckman Institute for Advanced Science and Technology, Urbana, IL 61801*

Received 7 March 2016; revised 26 April 2016; accepted 28 April 2016
Published online 4 May 2016 in Wiley Online Library (wileyonlinelibrary.com). DOI 10.1002/bip.22868

translocation 易位

ABSTRACT:

Calcium ions (Ca^{2+}) play key roles in various fundamental biological processes such as cell signaling and brain function. Molecular dynamics (MD) simulations have been used to study such interactions, however, the accuracy of the Ca^{2+} models provided by the standard MD force fields has not been rigorously tested. Here, we assess the performance of the Ca^{2+} models from the most popular classical force fields AMBER and CHARMM by computing the osmotic pressure of model compounds and the free energy of DNA–DNA interactions. In the simulations performed using the two standard models, Ca^{2+} ions are seen to form artificial clusters with chloride, acetate, and phosphate species; the osmotic pressure of $CaAc_2$ and $CaCl_2$ solutions is a small fraction of the experimental values for both force fields. Using the standard parameterization of Ca^{2+} ions in the simulations of Ca^{2+}-mediated DNA–DNA interactions leads to qualitatively wrong outcomes: both AMBER and CHARMM simulations suggest strong inter-DNA attraction whereas, in experiment, DNA molecules repel one another. The artificial attraction of Ca^{2+} to DNA phosphate is strong enough to affect the direction of the electric field-driven translocation of DNA through a solid-state nanopore. To address these shortcomings of the standard Ca^{2+} model, we introduce a custom model of a hydrated Ca^{2+} ion and show that using our model brings the results of the above MD simulations in quantitative agreement with experiment. Our improved model of Ca^{2+} can be readily applied to MD simulations of various biomolecular systems, including nucleic acids, proteins and lipid bilayer membranes. © 2016 Wiley Periodicals, Inc. Biopolymers 105: 752–763, 2016.

Keywords: *calcium; molecular dynamics; AMBER; CHARMM; force field; nucleic acid*

This article was originally published online as an accepted preprint. The "Published Online" date corresponds to the preprint version. You can request a copy of any preprints from the past two calendar years by emailing the Biopolymers editorial office at biopolymers@wiley.com.

INTRODUCTION

The calcium ion (Ca^{2+}) is an important secondary messenger in eukaryotic cell signaling that affects various vital functions such as development, homeostasis, neural activity, and immunity.[1–6] In the nucleus of eukaryotic cells, Ca^{2+} is known to play an important role in gene regulation[7,8] and in the case of neurons, brain function and memory.[9] In prokaryotic cells, Ca^{2+} concentration is precisely regulated because of its broad effects on development and proliferation.[10] In eukaryotic

Additional Supporting Information may be found in the online version of this article.

This work was supported in part by the National Science Foundation grant PHY-1430124, National Institutes of Health grant R01-HG007406 and Oxford Nanopore Technologies, Inc.

Correspondence to: Aleksei Aksimentiev; e-mail: aksiment@illinois.edu

organisms, calcium is a critical component of the muscle contraction cycle and failure in calcium signaling can cause cardiovascular diseases such as hypertension and heart failure.[2] At the molecular level, Ca^{2+} ions interact electrostatically with acidic patches of proteins (e.g., EF hand motif),[11] anionic lipids (e.g., phosphatidylinositol),[12–14] and nucleic acids.[15] Because of their $+2e$ electrical charge, divalent cations such as Ca^{2+} and Mg^{2+} coordinate nearby electronegative atoms, e.g., water, acetate (Ac^-), or phosphate oxygen atoms, more strongly than monovalent cations do.[16]

Ca^{2+} ions can bind to biomolecules in two distinct binding modes. Direct binding occurs in an environment that is relatively devoid of water molecules, such as in the binding pockets of proteins, RNA or chelators, where multiple negatively charged chemical groups, such as acetate and phosphate, form direct contacts with a Ca^{2+} ion. Direct binding tightly embeds a Ca^{2+} ion to a specific site and is known to play a role in the structural stability of RNA and proteins.[17,18] Structural biology techniques such as X-ray crystallography can elucidate the location of such directly bound, structural, Ca^{2+} ions, providing reliable initial molecular configurations for atomistic molecular dynamics (MD) simulations.

In an aqueous environment, solvated Ca^{2+} ions interact non-specifically with negatively charged species (e.g., phosphate groups of DNA and lipid) through bonds mediated by water molecules, an interaction that we refer to hereafter as indirect binding.[19] Experimental characterization of the diffuse ionic atmosphere formed by solvated Ca^{2+} ions around an oppositely charged biomolecule is difficult because of the transient nature of the interactions. Bai et al. counted the numbers (not positions) of individual cationic species in the ionic atmosphere of a DNA duplex, revealing that Ca^{2+} ions bind to DNA at least an order of magnitude stronger than monovalent cations do.[20] For example, a DNA duplex submerged in an electrolyte solution containing either 1 m*M* Ca^{2+} or 20 m*M* Na^+ will be surrounded by the same amount of ions. Due to their high affinity to DNA, Ca^{2+} ions can considerably reduce the electrostatic repulsion between DNA molecules. For example, the internal pressure of a DNA array is 20 bar at 250 m*M* NaCl but only 3 bar at 25 m*M* $CaCl_2$ at the same average nearest-neighbor distance (~30 Å) between the DNA molecules.[15] The high affinity of solvated Ca^{2+} to phosphate groups can also affect the structure and mechanical properties of lipid bilayer membranes. For example, increasing concentrations of Ca^{2+} make lipid membranes more rigid by promoting lipid tail ordering.[21,22]

Complementing experimental studies, the MD method has been used to elucidate the biological role of Ca^{2+} and other divalent cations.[23–30] In the framework of non-polarizable force fields such as AMBER and CHARMM, the models of divalent cations were developed to match the experimental solvation free energies of individual cations.[23,24] Recent simulations of the osmotic pressure of model solutions have shown that such non-polarizable models of divalent cations may not be accurate enough to properly describe the interactions of the cations with anions.[29,31,32] For example, we have previously shown that the attractive interaction of a Mg^{2+} ion with either a chloride (Cl^-), acetate, or phosphate anion is significantly overestimated in both CHARMM and AMBER force fields.[29] Similarly, Saxena and Garcia found their custom multi-site models of Mg^{2+} and Ca^{2+} ions to overestimate the attraction of the ions to chloride when the latter was described using the standard CHRAMM force field.[31,32]

Here, we examine the ability of popular MD force fields AMBER and CHARMM to describe the interaction of solvated Ca^{2+} ions with several representative anionic species: chloride, acetate, and phosphate. We find that the binding affinity of Ca^{2+} to all three anionic species is overestimated in both AMBER and CHARMM, causing artificial aggregation and clustering of the solutes. Following that, we describe an improved model of hydrated Ca^{2+} ions parameterized to reproduce experimental osmotic pressure data. Finally, we show that using our model of Ca^{2+} dramatically improves the realism of the MD simulations of DNA–DNA interactions and of Ca^{2+}-mediated electrophoretic motion of DNA through a solid-state nanopore.

RESULTS

Standard Parameterization of the CHARMM and AMBER Force Fields Overestimates Attraction of Ca^{2+} Ions to Biological Anions

To determine how accurate an all-atom MD simulation is in describing the interactions of Ca^{2+}–Cl^- and Ca^{2+}–Ac^- solute pairs, we simulated solutions of the binary mixtures ($CaCl_2$ or $CaAc_2$), measured the dependence of the osmotic pressure on the solute concentration, and compared the result with experimental osmotic pressure data. Following the protocols described in the previous studies,[29,33–36]the osmotic pressure was simulated using a two-compartment setup, Figures 1A and 1B. Briefly, the simulation box was divided into two compartments ("solute" and "water") by means of two half-harmonic potential walls (dashed lines in Figures 1A and 1B), that acted on the heavy atoms of solutes only. In equilibrium, the solute compartment is pressurized due to osmosis. The osmotic pressure is determined by measuring forces exerted by the solutes on the walls. The Materials and Methods section provides a more detailed description of the simulation procedures.

Our osmotic pressure simulations of the $CaAc_2$ solution using the standard MD force fields (both CHARMM and AMBER) showed considerable deviation between the

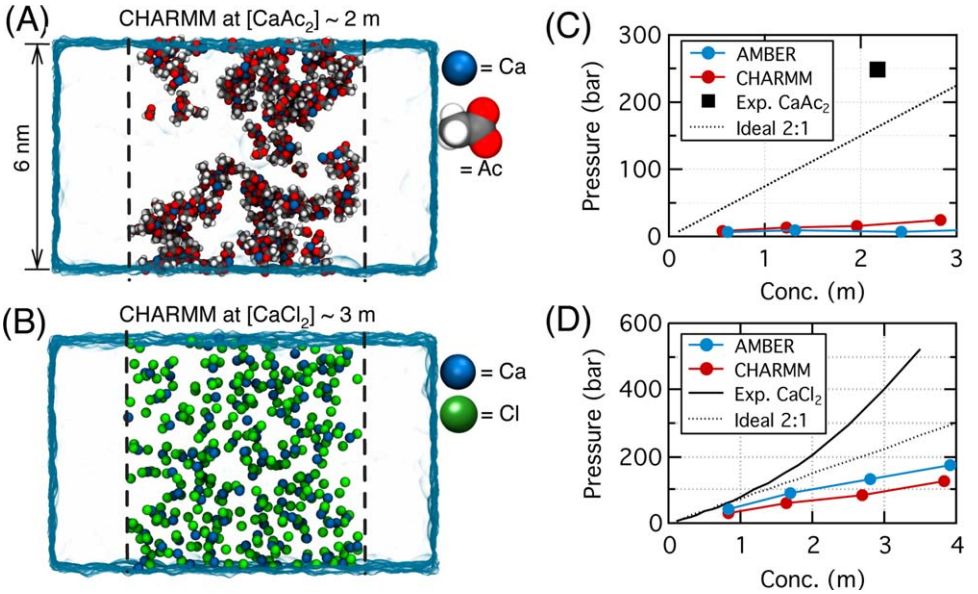

FIGURE 1 Standard molecular force fields overestimate association of Ca^{2+} with anionic species. (A,B) Representative configuration of solutes in MD simulations of 2 *m* $CaAc_2$ (A) and 3 *m* $CaCl_2$ (B) solutions performed using the standard CHARMM force field.[37] Only a 1 nm wide slice through the system is shown for clarity. In each panel, the blue semi-transparent surface illustrates the dimensions of a unit simulation cell; dashed lines indicate the presence of ideal semi-permeable membranes that confine solutes to one of the two compartments; the other compartment contains pure water. (C,D) Comparison of experimental (black square[38] or black line[39]) and simulated (red or blue) osmotic pressure values for the $CaAc_2$ (C) and $CaCl_2$ (D) solutions as a function of the solutes' concentration. The data were obtained using the standard AMBER (blue) and CHARMM (red) parameter sets. The osmotic pressure of an ideal 2:1 solution (osmotic coefficient = 1) is shown using dotted lines. The standard error of 1 ns block averages of 2 ps sampled osmotic pressure data are smaller than the symbols.

simulation outcomes and experiment.[38] Extensive cluster formation was observed in the simulations of the $CaAc_2$ solution using both force fields, Figure 1A. Such excessive cluster formation results in significant underestimation of the osmotic pressure at any solute concentration below the solubility limit (~2.2 *M* at room temperature). At ~2 *m*, the osmotic pressure was an order of magnitude smaller than the experimental value[38] for both force fields, Figure 1C. Although the only direct experimental measurement of the osmotic pressure is available for a fixed ~2 *m* concentration of $CaAc_2$, at lower concentrations the osmotic pressure should be larger than that of an ideal 2:1 solution (dotted line in Figure 1C).[39,40] At ~0.5 *m*, the simulated osmotic pressure was one fifth of the ideal value, Figure 1C. Given the fact that Ac^- is an essential chemical group of proteins and lipid membranes, the profound inaccuracy of the standard force field in the description of Ca^{2+}–Ac^- interaction warrants urgent improvement of the force field model.

In the case of a $CaCl_2$ solution, our MD simulations revealed inaccuracies of the standard CHARMM and AMBER force fields comparable to those of the $CaAc_2$ solutions. Ca^{2+} and Cl^- ions were seen to form direct pairs, leading to clustering, Figure 1B, and significant underestimation of the osmotic pressure, Figure 1D. At ~0.8 *m*, the simulated osmotic pressure was ~50–70% of the experimental value, depending on the force field used, Figure 1D. The discrepancy between the simulated and experimental osmotic pressure increased with the solute concentration, Figure 1D. At ~3 *m*, the simulated osmotic pressure was ~20–30% of the experimental value.

To evaluate the interactions of Ca^{2+} with phosphates, we computed the interaction free energy and the effective force between two parallel double stranded DNA (dsDNA) molecules. Experimentally, the interaction free energy of an array of aligned dsDNA molecules was quantitatively characterized at a 25 m*M* $CaCl_2$ solution using an osmotic pressure setup.[15] We have previously shown that the interaction free energy of a pair of parallel dsDNA molecules is directly related to the experimentally measured osmotic pressure of a DNA array[41] and can be used as a target for improvement of the MD force field.[34]

To compute the interaction free energy of a pair of parallel dsDNA molecules, we constructed a system containing two effectively infinite dsDNA molecules submerged in a 25 m*M*

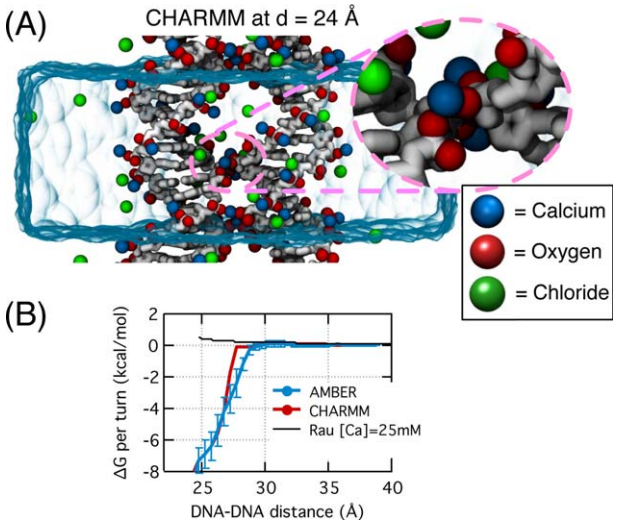

FIGURE 2 MD simulation of Ca^{2+}-mediated DNA–DNA interaction free energy using the standard CHARMM and AMBER force fields. (A) Representative configuration of DNA and ions in umbrella sampling simulations of the DNA–DNA potential of mean force. The DNA molecules are shown in gray. A blue semi-transparent surface depicts the volume occupied by the solvent in a unit simulation cell. Colored spheres indicate the locations of calcium (blue), phosphate oxygen (red) and chloride (green). This particular image shows the DNA system at an inter-DNA distance of 24 Å; the bulk concentration of $CaCl_2$ is 25 m*M*. The inset shows a pair of phosphate groups stabilized by multiple Ca^{2+} ions directly bound to the phosphates forming an ion bridge between the two DNA molecules. (B) The interaction free energy of two parallel dsDNA molecules versus the DNA–DNA distance at 25 m*M* $CaCl_2$ computed using the standard parameterization of the CHARMM (red) and AMBER (blue) force fields. The experimental dependence is shown as a black line.[15]

solution of $CaCl_2$, Figure 2A. The interaction free energy, ΔG, as a function of the inter-axial distance, d, was computed using the conventional umbrella sampling and weighted histogram analysis methods[42] see Materials and Methods for details. In our simulations using the standard force fields (CHARMM or AMBER), we observed direct pair formation between Ca^{2+} and phosphate oxygen atoms. The inset of Figure 2A demonstrates a representative configuration of Ca^{2+} ions forming ion "bridges" between two dsDNA molecules at $d = 24$ Å. Such direct binding of Ca^{2+} ions induces strong Ca^{2+}-mediated inter-DNA (or inter-phosphate) attraction, indicated by a sharp decrease of the DNA–DNA free energy at $d <\sim 28$ Å, which was observed for both force field models, Figure 2B. Thus, the simulated pairwise free energy suggests strong attraction between two dsDNA molecules, which is in qualitative disagreement with experimental measurements that show that DNA–DNA interaction is repulsive.[15] Quantitatively, the experimental ΔG at $d = 25$ Å was measured to be ~0.4 kcal/mol per DNA turn, whereas the simulation suggests a much greater and opposite sign value: −6 kcal/mol per turn, Figure 2B. In both experiment and simulation, ΔG is set to zero at large DNA–DNA separations.

Improved Model of a Ca^{2+} Heptahydrate Complex

To improve the parameterization of hydrated Ca^{2+} ions, we consider a Ca^{2+} heptahydrate complex, $Ca^{2+}(H_2O)_7$, that consists of one Ca^{2+} ion described using the CHARMM parameter set[24] and seven TIP3P water molecules[43] with modified dipole moments, Figure 3. In doing so, we limit the applicability of our model to systems where Ca^{2+} ions can be expected to remain fully hydrated. In the case of $CaCl_2$, X-ray absorption fine structure (XAFS) spectroscopy,[44,45] large-angle X-ray scattering (LAXS),[25] and neutron diffraction[46] have shown that Ca^{2+} and Cl^- ions do not form direct contacts at room temperature even at $CaCl_2$ concentrations as high as 6 m. For Ac^-, formation of a direct contact pair with Ca^{2+} is also unlikely because the osmotic pressures of $CaAc_2$ and $CaCl_2$ are comparable: 240 and 250 bar at 2.2 *m* of $CaAc_2$ and $CaCl_2$, respectively.[38,39] Experimental DNA array pressure measurements in 25 m*M* $MgCl_2$ and $CaCl_2$ solutions are quantitatively similar.[15] Previously, we have shown that simulated pressure of a DNA array in $MgCl_2$ can be matched with experiment only in the absence of direct contacts between Mg^{2+} ions and DNA phosphates.[29] Thus, it is reasonable to expect that the number of direct contacts between Ca^{2+} and DNA phosphates is negligible as well.

Although the exact number of water molecules coordinating a Ca^{2+} ion is not known, quantum calculations[47] and Car-Parrinello MD simulations[28,48] suggest a range of 7–8 and 6–8, respectively, whereas the coordination number of Ca^{2+} in the

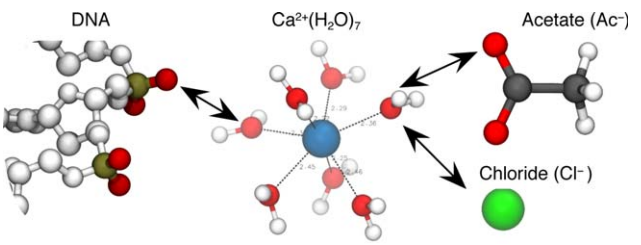

FIGURE 3 Reparameterization of a hydrated calcium ion using a heptahydrate model. In each heptahydrate complex, $Ca(H_2O)_7$, seven water oxygens are harmonically restrained to a calcium atom. To account for Ca^{2+}-induced polarization of water molecules,[47,48] the dipole moment of each of the seven water molecules in the heptahydrate complex is increased by 0.5 debye by adjusting the partial charges of water oxygen and water hydrogen atoms. Following that, the LJ σ parameters describing specific interactions between water oxygens of $Ca^{2+}(H_2O)_7$ and the target anionic species (phosphate oxygen, acetate oxygen, and Cl^-) are refined to match the experimental osmotic pressure data.

standard CHARMM force field is 7.[24] Because we base our model on the CHARMM force field model of Ca^{2+}, using seven water molecules to form a hydrated Ca^{2+} ion complex comes as a natural choice. Furthermore, independent simulation studies based on the AMOEBA polarizable model[27,49] and the Car-Parrinello model,[50] as well as EXAFS[45] and neutron diffraction[46] experiments, also predict the hydration number of a Ca^{2+} ion to be 7.

To distinguish the seven water molecules forming the $Ca^{2+}(H_2O)_7$ complex from bulk water, we prevent exchange of water molecules between the $Ca^{2+}(H_2O)_7$ complex and bulk water. Following the strategy applied to the Mg^{2+}-hexahydrate model,[29] we use a half-harmonic restraining potential between Ca^{2+} and water oxygens with a 3.0 Å equilibrium distance and a 50,000 kJ/(mol·nm^2) force constant to ensure that all seven water molecules remain in the complex with Ca^{2+}. Because the equilibrium distance between Ca^{2+} and water oxygen is ~2.5 Å, the potential exerts force on the restraining oxygen only when the atom attempts to escape from the complex. Because such restraints neither altered the equilibrium Ca–O distance nor the vibration dynamics of water, the effects of using such a restraining potential on the outcome of an MD simulation is negligible under the assumption that the ions remain fully hydrated.

According to the results of MD simulations employing a polarizable AMOEBA force field or the Car-Parrinello scheme,[48,49] the dipole moment of water molecules forming the first solvation shell of a divalent cation is ~0.5 debye larger than that of a bulk water molecule. To account for this polarization effect in the framework of a non-polarizable force field, we increased the dipole moments of water molecules in each $Ca^{2+}(H_2O)_7$ complex by 0.5 debye by changing the charge of the oxygen atom from $-0.834e$ to $-1.012e$ and the charge of each hydrogen atom from $0.417e$ to $0.506e$. A similar approach was used in our previous parameterization of the Mg^{2+} hexahydrate complex,[29] where increasing the dipole moment of the first solvation shell water molecules was found to be essential to match the osmotic pressure data.

Atom Pair-Specific Lennard-Jones Parameters Describing Interactions of $Ca^{2+}(H_2O)_7$ with Anionic Species

With all Ca^{2+} ions replaced by our $Ca^{2+}(H_2O)_7$ complexes, we recomputed the osmotic pressure of a 2 *m* $CaAc_2$ solution using both standard CHARMM and AMBER force fields. The replacement improved the agreement between simulation and experiment, increasing the osmotic pressure from 10–20 to 50 bar for both force fields, Supporting Information Figures S1A,B. To further refine the interaction between $Ca^{2+}(H_2O)_7$ and Ac^-, we gradually increased the Lennard-Jones (LJ) σ parameter for the $Ca^{2+}(H_2O)_7$ oxygen and Ac^- oxygen pairs, Figure 3, which is similar to the approach we previously used to refine the parameters of Mg^{2+} .[29] As σ increased, the simulated osmotic pressure monotonically increased as well, approaching the experimental value (~250 bar)[38] at $\Delta\sigma = 0.07$ Å for both force fields, Supporting Information Figures S1A,B.

Next, we repeated the same procedure for a 3 *m* $CaCl_2$ solution, Supporting Information Figure S2. In the case of $CaCl_2$, simple replacement of Ca^{2+} ions with $Ca^{2+}(H_2O)_7$ dramatically improved agreement between simulated and experimental osmotic pressure values, Supporting Information Figures S2A,B. Full agreement between simulation and experiment was observed when the LJ σ parameter for the $Ca^{2+}(H_2O)_7$ oxygen and Cl^- pairs was increased by 0.01 Å for both force fields, Supporting Information Figures S2A,B.

The dramatic improvements of the all-atom model in describing the osmotic pressure of $CaAc_2$ and $CaCl_2$ solutions result from the prevention of direct ion pair formation. In contrast to molecular configurations obtained using the standard parameterization, Figures 2A and 2B, the use of our $Ca^{2+}(H_2O)_7$ model results in a homogeneous distribution of the solutes within the solute compartment, Figures 4A and 4B. Recomputing the osmotic pressure of the two solutions for a full range of solute concentration reveals excellent agreement between the simulations carried out using our $Ca^{2+}(H_2O)_7$ model and experiment, Figures 4C and 4D.

Parameterization of the Hydrated Ca^{2+} Ion Interaction with DNA

Finally, we recomputed the free energy, ΔG, of two parallel dsDNA molecules as a function of the inter-DNA distance after having all Ca^{2+} ions replaced by our $Ca^{2+}(H_2O)_7$ complexes. Because acetate and phosphate oxygen atoms are chemically similar (note that both CHARMM and AMBER force fields use identical LJ parameters for both oxygen types), it is reasonable to assume that using parameters optimized for a $CaAc_2$ solution to describe interactions between oxygens of $Ca^{2+}(H_2O)_7$ and DNA phosphate will improve the overall agreement between simulated and experimental free energy of DNA–DNA interactions. Indeed, ΔG computed using the LJ σ correction for $CaAc_2$ was in a much better agreement with experiment than the original ΔG curve, Figures 5A and 5B. However, the resulting dependence of ΔG on the inter-DNA distance was too repulsive in comparison to the experimental one, indicating that the nonbonded interactions between Ca^{2+} and phosphate and between Ca^{2+} and acetate are different. To refine the interaction between $Ca^{2+}(H_2O)_7$ and DNA phosphate groups, we further adjusted the LJ σ parameter for the $Ca^{2+}(H_2O)_7$ water

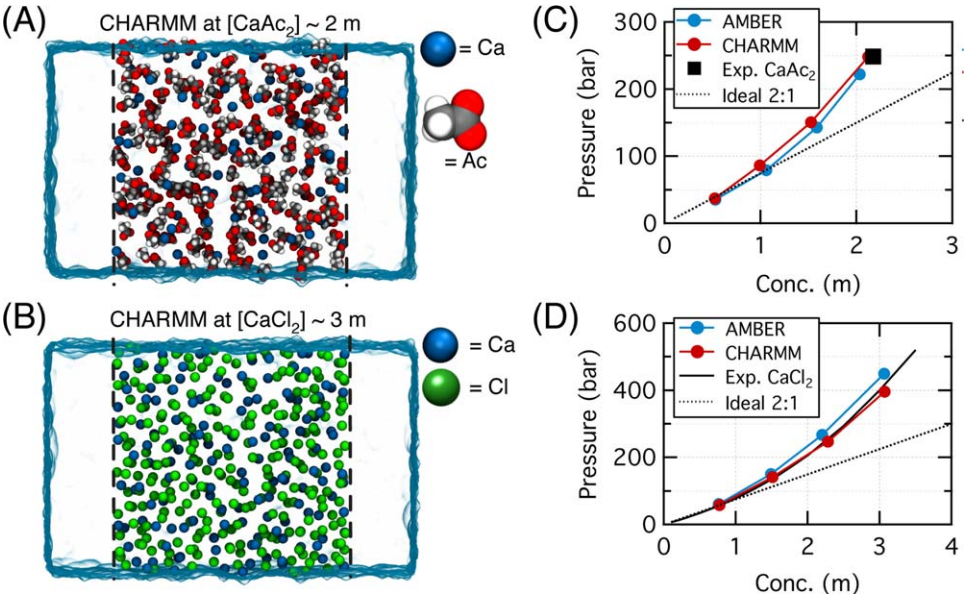

FIGURE 4 MD simulations of $CaAc_2$ and $CaCl_2$ solutions using the refined force field models. (A,B) Representative configuration of solutes in MD simulations of 2 *m* $CaAc_2$ (A) and 3 *m* $CaCl_2$ (B) solutions performed using our improved parameterization of Ca^{2+} ions. In each panel, the blue semi-transparent surface illustrates the dimensions of a unit simulation cell; dashed lines indicate the presence of ideal semi-permeable membranes that confine the solutes to one of the two compartments; the other compartment contains pure water. Only a 1 nm-wide slice of the system is shown for clarity. (C,D) Comparison of experimental (black square[38] or black line[39]) and simulated (red or blue) osmotic pressure values for the $CaAc_2$ (C) and $CaCl_2$ (D) solutions as a function of the solute concentration. The data were obtained using our calcium heptahydrate parameterization of Ca^{2+} ions in AMBER (blue) and CHARMM (red) force fields. The osmotic pressure of an ideal 2:1 solution (osmotic coefficient = 1) is shown using dotted lines. The standard error of 1 ns block averages of 2 ps sampled osmotic pressure data are smaller than the symbols.

oxygen and phosphate oxygen pairs. Increasing the LJ σ parameters by only 0.02 and 0.04 Å with respect to the standard value for the CHARMM and AMBER force fields, respectively, yielded the best agreement of the ΔG curve with experimental data for both force fields, Figures 5A and 5B.

Figure 5C shows a typical configuration of the two DNA system at $d = 24$ Å simulated using our optimized $Ca^{2+}(H_2O)_7$ model. Unlike the conformations obtained using the standard force fields, Figure 2A, there are no direct contacts between DNA and Ca^{2+} in the simulation carried out using our optimized parameters. Furthermore, Cl^- ions are almost completely excluded from the volume surrounding the DNA. The excessive presence of Cl^- ions near DNA in the simulations performed using the standard force fields was caused by direct binding of Cl^- ions to Ca^{2+} ions bound to the phosphate groups of DNA, Figure 2A.

The Effect of Ca^{2+} Models on MD Simulations of DNA Translocation Through a Solid-State Nanopore

Optical detection of DNA translocation through a solid-state nanopore[51,52] allows for massive parallelization of the DNA translocation measurements, which is required to make nanopore sequencing of DNA practical. In one optical detection method, DNA and calcium sensitive dye are placed on one side of a membrane containing a nanopore, whereas the solution on the other side of the membrane contains calcium ions. An electric field is applied to drive calcium ions from one side of the membrane to the other through a nanopore. When Ca^{2+} ions reach the other side, they combine with the calcium sensitive dye and emit a fluorescent signal. However, the presence of DNA in the nanopore reduces the flow of calcium ions, which in turn reduces the fluorescence of the dyes. Thus, a measurement of the fluorescence intensity can report on the presence of DNA in the nanopore.[52]

To investigate the effect of our new Ca^{2+} parameterization on the outcome of simulations designed to reproduce optical detection of DNA translocation, we built two all-atom models containing the same nanopore in a Si_3N_4 membrane and a 36 bp fragment of DNA threaded through it, Figure 6A. The initial conformation of the DNA molecule along with any bound Ca^{2+} ions were obtained from separate equilibration simulations of DNA in a bulk electrolyte solution lasting hundreds of

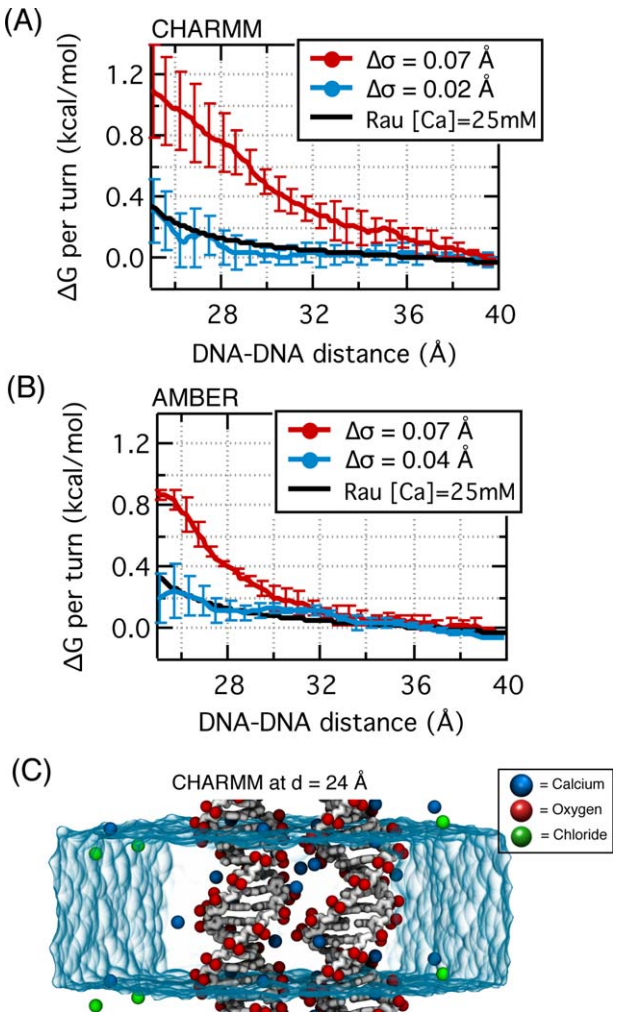

FIGURE 5 Simulations of DNA–DNA potential of mean force using our refinement of the CHARMM and AMBER force fields. (A,B) The interaction free energy of two parallel dsDNA molecules versus the DNA–DNA distance at 25 m*M* $CaCl_2$ computed using our refined parameterization of the CHARMM (A) and AMBER (B) force fields. The experimental dependence is shown as a black line.[15] The red lines show the results obtained using the same adjustments of the σ parameter for the $Ca^{2+}(H_2O)_7$ oxygen–DNA phosphate oxygen pair as for the $Ca^{2+}(H_2O)_7$ oxygen–Ac^- oxygen pair ($\Delta\sigma$=0.07 Å for both force fields). Blue lines show the results obtained using the σ parameters adjusted to reproduce experimental DNA–DNA interaction free energy ($\Delta\sigma$=0.02 and 0.04 Å for CHARMM and AMBER, respectively). (C) Representative configuration of DNA and ions in umbrella sampling simulations of the DNA–DNA PMF carried out using our refined version of the CHARMM force field. The DNA molecules are shown in gray, a blue semi-transparent surface depicts the volume occupied by the solvent in a unit simulation cell. Colored spheres indicate the locations of calcium (blue), phosphate oxygen (red) and chloride (green). This particular image shows the DNA system at the inter-DNA distance of 24 Å; the bulk concentration of $CaCl_2$ is 25 m*M*.

nanoseconds, see Materials and Methods for details. The systems were then solvated with a hexagonal prism volume of electrolyte solution containing 0.4 *M* KCl and 65 m*M* $CaCl_2$, typical conditions realized in experiment.[52] The only difference between the two systems was in the description of the hydrated Ca^{2+} ions: standard CHARMM parameterization was used for one system whereas the other system was described using our custom $Ca^{2+}(H_2O)_7$ model and the appropriate NBFIX corrections, Table I. After short energy minimization, both systems were equilibrated for 2 ns allowing them to attain an equilibrium volume. Each system was then simulated under applied electric field of different magnitudes, corresponding to a transmembrane bias of 1 V, 200 mV and 100 mV.

Figures 6B–6D characterize the displacement of the DNA strand in response to applied electric field. At 1 V, the choice of a calcium model determines the direction of DNA translocation: the standard CHARMM model predicts DNA translocation in the direction of the applied electric field, whereas our improved model indicates translocation in the direction opposite to the applied electric field, the latter being in agreement with experiment.[52] At lower biases, a more complex dependence is observed in the simulations performed using the standard CHARMM force field. At 200 mV, the DNA moves initially in the direction of the applied field but then reverses the translocation direction; at 100 mV, the DNA gradually moves along the direction of the applied electric field. In contrast, reducing the bias in the simulation carried out using our improved model of Ca^{2+} is seen to only reduce the overall speed of DNA translocation in proportion to the bias magnitude, without altering its direction.

The counterintuitive behavior observed in the CHARMM-based simulations is explained by overcharging of the DNA molecule. The equilibration simulations performed in a solution containing 65 m*M* of $CaCl_2$ and 400 m*M* of KCl resulted in 79 Ca^{2+} ions bound to a DNA molecule that contained only 70 phosphate groups, Supporting Information Figure S5. Furthermore, the Ca^{2+} binding to DNA did not show signs of saturation, and we expect that if the equilibration simulations were continued, many more Ca^{2+} would bind to the DNA, up to a maximum of nearly 140 Ca^{2+} ions (two Ca^{2+} per phosphate group). Without taking into account the secondary binding of Ca^{2+} to Cl^- ions, the DNA molecule and bound Ca^{2+} ions together had a charge of $+88e$ at the end of the equilibration simulation. When the equilibrated DNA molecule was transferred to the nanopore system along with the bound Ca^{2+} ions, the secondary bound Cl^- ions (i.e., Cl^- ions bound to Ca^{2+} ions bound to DNA) were not transferred and hence the DNA-Ca^{2+} construct was positively charged at the beginning of the nanopore simulations. In the applied field simulations, the complex initially moves in the direction of the

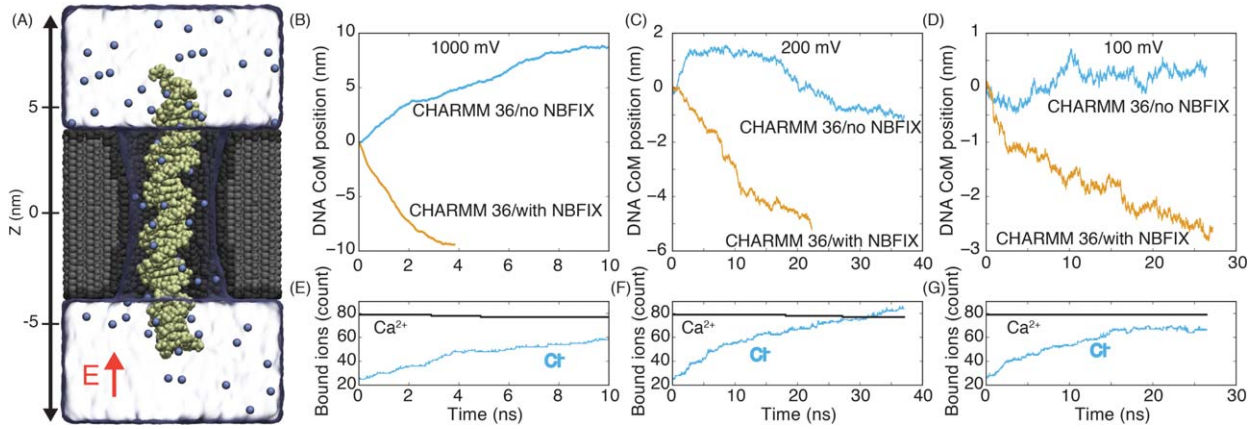

FIGURE 6 Simulations of electric field-driven nanopore transport of DNA in the presence of Ca^{2+} ions. (A) The microscopic configuration of the nanopore system at the beginning of the DNA translocation simulations. DNA is shown using tan spheres; calcium ions are shown as blue spheres. The volume occupied by water is indicated by a semi-transparent surface. The Si_3N_4 membrane is shown cut away, with surface atoms shown as black spheres and the interior atoms shown as grey spheres. In addition to calcium, the solution contains 0.4 *M* of KCl (not shown). The arrow illustrates the direction of applied electric field producing a positive transmembrane bias. (B-D) The *z* coordinate of the DNA's center of mass (CoM) during MD simulations at a transmembrane bias of 1 V (B), 200 mV (C), and 100 mV (D). Data from simulations performed using the standard parameterization of the CHARMM force field are shown in blue; orange lines illustrate the results of simulations performed using our parameterization of Ca^{2+} ions for the CHARMM force field. The *z* coordinate is defined in panel A. (E-G) The number of calcium ions directly bound to DNA (black) and the number of chloride ions directly bound to calcium ions that are already bound to DNA (blue) during the simulations of DNA translocation performed at a transmembrane bias of 1 V (E), 200 mV (F), and 100 mV (G). These data characterize the simulations carried out using the standard CHARMM force field. No Cl^-–Ca^{2+}–DNA binding (defined as a Cl^- ion remaining within 0.4 nm of a Ca^{2+} ion for more than 30 ps) was observed in MD simulations employing our parameterization of Ca^{2+} ions.

applied field. As the simulations progress, the number of bound calcium does not change, but the number of secondary bound Cl^- ions increases, Figures 6E–6G. At 1 V, the DNA escapes the nanopore before significant number of Cl^- ions binds to DNA. At 200 mV, the DNA translocation is considerably slower, so the DNA charge does become negative and the DNA reverses the direction of its motion. At 100 mV, the DNA charge is close to zero, leading to a small displacement in the applied electric field.

All of the above indicate that MD simulation of electric field-driven motion of DNA in the presence of Ca^{2+} done using the standard parameterization of the CHARMM force field leads to considerable artifacts, including outcomes that are in qualitative disagreement with experiment. In contrast, our model predicts DNA translocation behavior consistent with experimental observation, making computational studies of such systems and processes more realistic.

DISCUSSION

Because Ca^{2+} ions play a crucial role in cell signaling that occurs in the vicinity of cell membranes, the interaction of Ca^{2+} with lipid bilayers has been an important subject of MD simulations.[53] Several groups used MD simulations to investigate the effects of Ca^{2+} on the structure and organization of lipid bilayers, reporting Ca^{2+}-induced formation of clusters in anionic phosphatidylserine (PS)[13,54] and neutral

Table I Reparametrization of Lennard-Jones Interactions Between $Ca^{2+}(H_2O)_7$ Water Oxygen and Anionic Species (Cl^-, Acetate Oxygen, and Phosphate Oxygen)

Atom Type	$\sigma^{standard}$	$\Delta\sigma$	σ^{NBFIX}
CHARMM Cl^-	3.61	0.01	3.62
CHARMM acetate(O)	3.09	0.07	3.16
CHARMM phosphate(O)	3.09	0.02	3.11
AMBER Cl^-	3.81	0.01	3.82
AMBER acetate(O)	3.06	0.07	3.13
AMBER phosphate(O)	3.06	0.04	3.10

Listed are pair-specific adjustments to the LJ σ parameter, expressed as the difference ($\Delta\sigma$, Å) between the optimal value of this parameter for the specific ion pair and the standard value for that pair. The partial charges of the oxygen and hydrogen atoms within a $Ca^{2+}(H_2O)_7$ complex are $-1.012e$ and $0.506e$, respectively.

phosphatidylcholine (PC)[55,56] membranes. The force that drove such lipid clustering was the direct interaction of Ca^{2+} ions with phosphate (PC and PS) and acetate (PS) groups of multiple lipid molecules, which is similar to the artificial ion bridging observed in our simulations of two DNA molecules using the standard CHARMM force field, Figure 2A. Experimentally, lipid head groups are known to be highly hydrated.[57] Therefore, it is plausible that our $Ca^{2+}(H_2O)_7$ model of hydrated Ca^{2+} ions may provide a more realistic description of Ca^{2+} ions interaction with lipid bilayers than the standard parameterization of the CHARMM force field.

A potential drawback of our $Ca^{2+}(H_2O)_7$ model is that it does not allow a direct contact pair formation between Ca^{2+} and anionic species. As discussed in detail in one of the previous sections (see "Improved model of a Ca^{2+}-heptahydrate complex"), a number of experimental studies suggest that Ca^{2+} is unlikely to form a direct contact pair with acetate, phosphate, or Cl^- in an aqueous environment.[15,25,38–40,45,46] One can, however, imagine a situation where ability to simulate direct binding would be desirable, for example, in the simulations of a chelator function or allosteric change upon Ca^{2+} binding.[58] For such simulations, the MD code can be modified to allow for probabilistic exchange of water from the first solvation shell of a Ca^{2+} ion with an atom of a protein or a chelator. Development of such an algorithm is one of our future goals. An alternative approach is to use the multi-site model that allows for direct contact pair formation.[32] We should, however, point out that the latter model does not take the first solvation shell polarization into account nor has it been validated yet for simulations of systems containing acetate or phosphate groups.

It is important to note that our modifications to the dipole moments of the first solvation shell water molecules appear to be an efficient approach for implementation of polarization effects[59–61] within the framework of a non-polarizable model. Because such modifications affect Coulombic interactions of $Ca^{2+}(H_2O)_7$ or $Mg^{2+}(H_2O)_6$ with all other chemical groups, using hydrated models of multivalent ions may improve the description of multivalent ion interactions with a range of polar groups. We stress, however, that applications of our $Ca^{2+}(H_2O)_7$ model to systems not explicitly considered in the present work requires further validation of the model.

MATERIALS AND METHODS

General MD Methods

All MD simulations of model compound mixtures and inter-DNA free energy calculations were done using the Gromacs 4.5.5 package. The simulations employed a 2 fs time step for integration[62] and an 8–10 Å switching scheme to evaluate van der Waals forces. Electrostatic forces were computed using particle-Mesh Ewald (PME) summation[63] with a 12 Å cutoff for the real-space Coulomb interaction and a 1.2 Å Fourier-space grid spacing. Temperature was kept constant at 298 K using the Nosé-Hoover scheme[64,65]; pressure was kept constant at 1 bar using the Parrinello-Rahman scheme applied semi-isotropically.[66] In the simulations of the osmotic pressure, the *xy* area of the simulation systems (the area of the semi-permeable membranes) was kept constant but the systems were allowed to change their dimensions along the *z* axis to achieve the target pressure. In the free energy simulations, the systems' dimension along the DNA axis (*z* axis) was kept constant but the systems were allowed to change their dimensions along the *x* and *y* axes. SETTLE[67] and LINCS[68] algorithms were used to constrain covalent bonds to hydrogen atoms in water and non-water molecules, respectively.

All DNA translocation simulations were carried out using NAMD2,[69] with a 2 fs time step and periodic boundary conditions. Multiple timestepping was employed, with local interactions being calculated every time step, and full interactions calculated every three steps. The van der Waals forces were smoothly cut off from 10 to 12 Å. The particle mesh Ewald method was used to evaluate long-range electrostatic interactions[63] over 1.0 Å-resolution grids. SETTLE[67] and RATTLE[70] algorithms were applied to covalent bonds involving hydrogen atoms in water and DNA, respectively. The Nose-Hoover Langevin[71] piston scheme with a period of 400 fs and a damping time scale of 200 fs was used for pressure control in the NPT simulations. Temperature in bulk solution simulations was controlled by a Langevin thermostat with a damping constant of 0.5 ps^{-1}. Temperature in nanopore translocation simulations was controlled by a Langevin thermostat acting on the membrane atoms with a damping constant of 1.0 ps^{-1}; all simulations under applied electric field were carried out in a constant temperature, volume and number of particles (NVT) ensemble.

Force Fields

In this work, we considered both CHARMM and AMBER force fields.

The CHARMM parameters for DNA and Ac^- molecules were taken from the standard distribution of the CHARMM27 force field,[72] which includes ion parameters for Ca^{2+} [24] and Cl^-.[73] Although a newer version of DNA force field (CHARMM36) is now available,[74] the difference between the two force fields is in updated bonded parameters and therefore our updated parameterization of calcium-DNA interactions equally applies to both CHARMM27 and CHARMM36 parameters sets as the two have identical non-bonded parameters.

The AMBER parameters for DNA and Ac^- molecules were taken from the standard distribution featuring the AMBER99 parameter set[75,76] for biomolecules. The parameters for Cl^- were taken from the standard ion model developed by the Cheatham group for the AMBER force field.[77] Because parameters describing divalent ions in the standard AMBER force field[23] are known to be outdated,[77] we chose the Ca^{2+} model from the standard CHARMM force field[24] to be our baseline parameterization of Ca^{2+} for AMBER, which is a reasonable approximation because both AMBER and CHARMM parameters employ the same water model, TIP3P. In all simulations, we used the standard TIP3P model for water.[43]

The standard Lennard-Jones (LJ) parameters (σ and ϵ) for a pair of atoms were determined using the Lorentz-Berthelot mixing rule,

which is the standard method for both CHARMM and AMBER force fields. Corrections to the LJ σ parameter of a specific atom pair were introduced using the nonbond_params entry in the Gromacs parameter file or NBFIX entry in the CHARMM parameter file. The final set of corrections is summarized in Table I.

Protocol of Osmotic Pressure Simulations

Each simulation system contained two compartments separated by two virtual semi-permeable membranes aligned with the *xy* plane. One compartment contained an electrolyte solution while the other contained pure water. We modeled the semi-permeable membranes using a half-harmonic planar potential that applied to solute molecules only, making it invisible to water:

$$F_i^{\text{memb}} = \begin{cases} -k(z_i - D/2) & \text{for} \quad z_i > D/2 \\ 0 & \text{for} \quad |z_i| \le D/2 \\ -k(z_i + D/2) & \text{for} \quad z_i < -D/2 \end{cases} \tag{1}$$

where z_i is the z coordinate of ion i, D is the width of the electrolyte compartment, and the force constant $k = 4000$ kJ/(mol·nm^2). Such half-harmonic potentials were applied using the mdrun program of Gromacs 4.5.5 package.[62] During the simulations, we recorded the instantaneous force applied to both membranes by the solutes. The instantaneous pressure on the membranes was obtained by dividing the instantaneous total force on the membranes by the total area of the membranes.

For a given condition (solute concentration, adjustments to interaction parameters), we performed at least a 10 ns equilibration simulation, followed by a production run of at least 100 ns. The osmotic pressure of each system was computed by averaging the instantaneous pressure. Statistical uncertainty in determination of the osmotic pressure was characterized as the standard error of 1 ns block averages of instantaneous pressure. Further details can be found in the description of our previous study.[29]

Simulation Protocol for Computing DNA–DNA Interaction Free Energy

We used the conventional umbrella sampling and weighted histogram analysis method[42] to compute the interaction free energy between a pair of dsDNA molecules (dG_{10}·dC10). The DNA helices were parallel to the z axis and covalently bound to themselves across the periodic boundary of the system. The simulation box was a water-filled hexagonal prism, which was ~9 nm on a side within the *x*–*y* plane and 3.4 nm along the z axis. Specific ionic conditions were obtained by replacing randomly chosen water molecules with ions. Each system was equilibrated for at least 10 ns at a specific ionic condition.

Umbrella sampling simulations were performed on the equilibrated systems. The force constant of the harmonic umbrella potentials was 1,000 kJ/(mol·nm^2). The reaction coordinate was defined as the distance between the centers of mass of the DNA molecules projected onto the *xy* plane; the range of ξ in the umbrella sampling was 24–40 Å with 1 Å spacing. Per each window, we performed at least 10 ns of equilibration simulation followed by a production run of at least 100 ns. Thus, ~20-μs-long sampling was required to compute each individual free energy curve reported in this study. The weighted histogram analysis method was used for the reconstruction of free energy from the umbrella sampling simulations.[42] To estimate the error, we divided data in each window into four non-overlapping subsets, computed four free energy curves using the subsets, and calculated standard deviation of those four free energy curves.

Simulation of DNA Translocation Through a Solid-State Nanopore

To simulate transport of DNA through a solid-state nanopore, a $(ACTG)_9$ fragment of dsDNA was built using the 3D-DART server.[78] The DNA molecule was submerged in a cubic volume (14 nm on each side) of solution containing 0.4*M* KCl and 65 m*M* $CaCl_2$, which is a typical experimental solution used in optical detection of DNA translocation.[52] The system was equilibrated by restraining all DNA heavy atoms to their original positions with a spring constant of 1 kcal/(mol Å^2) for 1 ns, and then restraining only phosphorous atoms using the same spring constant for 1 ns, followed by a free equilibration simulation of 10 ns. To decrease the computational cost of subsequent equilibration runs, the DNA molecules along with all bound Ca^{2+} ions were placed in a rectangular volume (6 nm × 6 nm × 18 nm) filled with 0.4 *M* KCl and 65 m*M* $CaCl_2$ aqueous solution. The system was equilibrated for 1 ns applying harmonic restraints of 1 kcal/(mol Å^2) to all DNA heavy atoms and bound Ca^{2+} ions. Finally, the system was equilibrated for 490 ns under 1 kcal/(mol Å^2) harmonic restraints applied to each phosphorous atom of the DNA. During the equilibration, calcium ions were observed to permanently bind to DNA, Supporting Information Figure S5, which lowered their concentration in solution. To keep the calcium concentration in solution constant at 65 m*M*, randomly chosen water molecules were replaced with calcium and chloride ions during the 490 ns equilibration run; six such replacements occurred during the equilibration run.

The equilibrated DNA molecule along with all permanently bound Ca^{2+} ions (defined as being within 0.3 nm of any phosphate oxygen atoms) were placed inside a 3.5 nm diameter nanopore in a 7 nm thick silicon nitride membrane, Figure 6A. The nanopore was built following a previously described procedure[79]; the DNA axis was aligned with the nanopore axis to avoid direct contacts between DNA and the nanopore surface. Following that, the system was solvated to form a hexagonal prism volume 9 nm across and 19 nm in length. Potassium, calcium and chloride ions were added to bring the bulk concentration of ions to 0.4 *M* KCl and 65 m*M* $CaCl_2$. The system was equilibrated having the heavy atoms of DNA restrained for the first 2 ns of equilibration; during the first nanosecond, bound calcium ions were also restrained. Following that, the restraints on DNA were released and the system was simulated at constant volume conditions under external electric field producing a transmembrane bias of either 1.0 V, 200 mV, or 100 mV.[80]

A second nanopore system was built and simulated following the exact same procedures as above except that all Ca^{2+} ions were replaced by calcium heptahydrate complexes, $Ca^{2+}(H_2O)_7$, and that NBFIX corrections, Table I, were used to describe the interactions between $Ca^{2+}(H_2O)_7$ and Cl^- and DNA phosphates, Figure 3. The initial equilibration of DNA in bulk electrolyte containing 0.4 *M* KCl, and 65 m*M* $Ca^{2+}(H_2O)_7$ lasted ~100 ns, no long lasting binding of $Ca^{2+}(H_2O)_7$ to DNA (or Cl^-) was observed during the equilibration run or simulations of DNA translocation through the nanopore driven by an applied electric field.

In all simulations of the nanopore systems, surface atoms of the silicon nitride membrane were restrained using harmonic potentials of 10 kcal/(mol·Å^2) spring constants; the interior atoms were restrained using 1 kcal/(mol·Å^2) harmonic potentials to give the membrane a relative bulk permittivity of 7.5.[81] The interactions of silicon nitride atoms with the rest of the system were described by a custom force field.[80] All other interactions were governed by the CHARMM36 force field; previously described NBFIX corrections were applied to describe interactions of potassium ions with chloride ions and DNA phosphates.[29] A grid-based potential[82] was applied to prevent calcium ions from sticking to the surface of Si_3N_4.[81] The DNA was constrained to remain aligned along nanopore axis via a half-harmonic potential acting on the DNA phosphorous atoms; the onset of the half-harmonic potential began at 1.5 nm from the axis of the nanopore, and the spring constant was 1000 pN/nm.

ACKNOWLEDGMENTS

The authors acknowledge supercomputer time at the Blue Waters Sustained Petascale Facility (University of Illinois) and at the Texas Advanced Computing Center (Stampede, allocation award MCA05S028).

REFERENCES

1. Berridge, M. J. Nature 1993, 361, 315–325.
2. Berridge, M. J.; Bootman, M. D.; Roderick, H. L. Nat Rev Mol Cell Biol 2003, 4, 517–529.
3. Clapham, D. E. Cell 1995, 80, 259–268.
4. Clapham, D. E. Cell 2007, 131, 1047–1058.
5. McLaughlin, S.; Wang, J.; Gambhir, A.; Murray, D. Annu Rev Biophys Biomol Struct 2002, 31, 151–175.
6. McLaughlin, S.; Murray, D. Nature 2005, 438, 605–611.
7. Dolmetsch, R. E.; Lewis, R. S.; Goodnow, C. C.; Healy, J. I. Nature 1997, 386, 855–858.
8. Dolmetsch, R. E.; Xu, K.; Lewis, R. S. Nature 1998, 392, 933–936.
9. Bading, H. Nat Rev Neurosci 2013, 14, 593–608.
10. Dominguez, D. C. Mol Microbiol 2004, 54, 291–297.
11. Nakayama, S.; Kretsinger, R. H. Annu Rev Biophys Biomol Struct 1994, 23, 473–507.
12. Ellenbroek, W. G.; Wang, Y. H. H.; Christian, D. A.; Discher, D. E.; Janmey, P. A.; Liu, A. J Biophys J 2011, 101, 2178–2184.
13. Boettcher, J. M.; Davis-Harrison, R. L.; Clay, M. C.; Nieuwkoop, A. J.; Ohkubo, Y. Z.; Tajkhorshid, E.; Morrissey, J. H.; Rienstra, C. M. Biochemistry 2011, 50, 2264–2273.
14. Wang, Y. H.; Collins, A.; Guo, L.; Smith-Dupont, K. B.; Gai, F.; Svitkina, T.; Janmey, P. A. J Am Chem Soc 2012, 134, 3387–3395.
15. Rau, D. C.; Lee, B.; Parsegian, V. A. Proc Natl Acad Sci USA 1984, 81, 2621–2625.
16. Qiu, X.; Parsegian, V. A.; Rau, D. C. Proc Natl Acad Sci USA 2010, 107, 21482–21486.
17. Celander, D.; Cech, T. Science 1991, 251, 401–407.
18. Draper, D. E.; Grilley, D.; Soto, A. M. Annu Rev Biophys Biomol Struct 2005, 34, 221–243.
19. Sotomayor, M.; Schulten, K. Biophys J 2008, 94, 4621–4633.
20. Bai, Y.; Greenfeld, M.; Travers, K. J.; Chu, V. B.; Lipfert, J.; Doniach, S.; Herschlag, D. J Am Chem Soc 2007, 129, 14981–14988.
21. Pabst, G.; Hodzic, A.; Strancar, J.; Danner, S.; Rappolt, M.; Laggner, P. Biophys J 2007, 93, 2688–2696.
22. Sovago, M.; Wurpel, G. W. H.; Smits, M.; Müller, M.; Bonn, M. J Am Chem Soc 2007, 129, 11079–11084.
23. Åqvist, J. J Phys Chem 1990, 94, 8021–8024.
24. Marchand, S.; Roux, B. Proteins: Struct, Funct, Bioinf 1998, 33, 265–284.
25. Jalilehvand, F.; Spångberg, D.; Lindqvist-Reis, P.; Hermansson, K.; Persson, I.; Sandström, M. J Am Chem Soc 2001, 123, 431–441.
26. Sponer, J.; Leszczynski, J.; Hobza, P. Biopolymers 2001, 61, 3–31.
27. Piquemal, J. P.; Perera, L.; Cisneros, G. A.; Ren, P.; Pedersen, L. G.; Darden, T. A. J Chem Phys 2006, 125, 054511.
28. Ikeda, T.; Boero, M.; Terakura, K. J Chem Phys 2007, 127, 074503.
29. Yoo, J.; Aksimentiev, A. J Phys Chem Lett 2012, 3, 45–50.
30. Yoo, J.; Aksimentiev, A. J Phys Chem B 2012, 116, 12946–12954.
31. Saxena, A.; Sept, D. J Chem Theory Comput 2013, 9, 3538–3542.
32. Saxena, A.; García, A. E. J Phys Chem B 2015, 119, 219–227.
33. Luo, Y.; Roux, B. J Phys Chem Lett 2009, 1, 183–189.
34. Yoo, J.; Aksimentiev, A. J Chem Theory Comput 2016, 12, 430–443.
35. Miller, M.; Lay, W.; Elcock, A. H. J Phys Chem B 2016, In press. DOI: 10.1021/acs.jpcb.6b01902.
36. Lay, W. K.; Miller, M. S.; Elcock, A. H. J Chem Theory Comput 2016, 12, 1401–1407.
37. Best, R. B.; Zhu, X.; Shim, J.; Lopes, P. E. M.; Mittal, J.; Feig, M.; MacKerell, A. D. Jr., J Chem Theory Comput 2012, 8, 3257–3273.
38. Apelblat, A.; Korin, E. J Chem Thermodynamics 2001, 33, 113–120.
39. Robinson, R. A.; Stokes, R. H. Electrolyte Solutions; Butterworths scientific publications, London, 1959.
40. Dill, K. A.; Bromberg, S. Molecular Driving Forces: Statistical Thermodynamics in Biology, Chemistry, Physics, and Nanoscience; Garland Science, New York, 2010.
41. Yoo, J.; Aksimentiev, A. Nucleic Acids Res 2016, 44, 2036–2046.
42. Kumar, S.; Rosenberg, J. M.; Bouzida, D.; Swendsen, R. H.; Kollman, P. A. J Comput Chem 1992, 13, 1011–1021.
43. Jorgensen, W. L.; Chandrasekhar, J.; Madura, J. D.; Impey, R. W.; Klein, M. L. J Chem Phys 1983, 79, 926–935.
44. Fulton, J. L.; Heald, S. M.; Badyal, Y. S.; Simonson, J. M. J Phys Chem A 2003, 107, 4688–4696.
45. Fulton, J. L.; Chen, Y.; Heald, S. M.; Balasubramanian, M. J Chem Phys 2006, 125, 094507.
46. Badyal, Y. S.; Barnes, A. C.; Cuello, G. J.; Simonson, J. M. J Phys Chem A 2004, 108, 11819–11827.
47. Schwenk, C. F.; Loeffler, H. H.; Rode, B. M. J Chem Phys 2001, 115, 10808–10813.
48. Bakó, I.; Hutter, J.; Pálinkás, G. J Chem Phys 2002, 117, 9838–9843.
49. Jiao, D.; King, C.; Grossfield, A.; Darden, T. A.; Ren, P. J Phys Chem B 2006, 110, 18553–18559.

50. Lightstone, F. C.; Schwegler, E.; Allesch, M.; Gygi, F.; Galli, G. ChemPhysChem 2005, 6, 1745–1749.
51. McNally, B.; Singer, A.; Yu, Z.; Sun, Y.; Weng, Z.; Meller, A. Nano Lett 2010, 10, 2237–2244.
52. Ivankin, A.; Henley, R. Y.; Larkin, J.; Carson, S.; Toscano, M. L.; Wanunu, M. ACS Nano 2014, 8, 10774–10781.
53. Maffeo, C.; Bhattacharya, S.; Yoo, J.; Wells, D. B.; Aksimentiev, A. Chem Rev 2012, 112, 6250–6284.
54. Pedersen, U. R.; Leidy, C.; Westh, P.; Peters, G. H. Biochim Biophys Acta Biomembr 2006, 1758, 573–582.
55. Böckmann, R. A.; Grubmüller, H. Angew Chem Int Ed Engl 2004, 43, 1021–1024.
56. Issa, Z. K.; Manke, C. W.; Jena, B. P.; Potoff, J. J. J Phys Chem B 2010, 114, 13249–13254.
57. Berger, O.; Edholm, O.; Jähnig, F. Biophys J 1997, 72, 2002–2013.
58. Luan, B.; Carr, R.; Caffrey, M.; Aksimentiev, A. Proteins: Struct, Funct, Bioinf 2010, 78, 1162.
59. Baker, C. M.; Lopes, P. E. M.; Zhu, X.; Roux, B.; MacKerell, A. D., Jr., J Chem Theory Comput 2010, 6, 1181–1198.
60. Ponder, J. W.; Wu, C.; Ren, P.; Pande, V. S.; Chodera, J. D.; Schnieders, M. J.; Haque, I.; Mobley, D. L.; Lambrecht, D. S.; DiStasio, R. A.; Head-Gordon, M.; Clark, G. N. I.; Johnson, M. E.; Head-Gordon, T. J Phys Chem B 2010, 114, 2549–2564.
61. Li, H.; Ngo, V.; Da Silva, M. C.; Salahub, D. R.; Callahan, K.; Roux, B.; Noskov, S. Y. J Phys Chem B 2015, 119, 9401–9416.
62. Hess, B.; Kutzner, C.; van der Spoel, D.; Lindahl, E. J Chem Theory Comput 2008, 4, 435–447.
63. Darden, T. A.; York, D.; Pedersen, L. J Chem Phys 1993, 98, 10089–10092.
64. Nose, S.; Klein, M. L. Mol Phys 1983, 50, 1055–1076.
65. Hoover, W. G. Phys Rev A 1985, 31, 1695–1697.
66. Parrinello, M.; Rahman, A. J Appl Phys 1981, 52, 7182–7190.
67. Miyamoto, S.; Kollman, P. A. J Comput Chem 1992, 13, 952–962.
68. Hess, B.; Bekker, H.; Berendsen, H. J. C.; Fraaije, J. G. E. M. J Comput Chem 1997, 18, 1463–1472.
69. Phillips, J. C.; Braun, R.; Wang, W.; Gumbart, J.; Tajkhorshid, E.; Villa, E.; Chipot, C.; Skeel, R. D.; Kale, L.; Schulten, K. J Comput Chem 2005, 26, 1781–1802.
70. Andersen, H. C. J Comput Phys 1983, 52, 24–34.
71. Martyna, G. J.; Tobias, D. J.; Klein, M. L. J Chem Phys 1994, 101, 4177–4189.
72. MacKerell, A. D., Jr.; Banavali, N. K. J Comput Chem 2000, 21, 105–120.
73. Beglov, D.; Roux, B. J Chem Phys 1994, 100, 9050–9063.
74. Hart, K.; Foloppe, N.; Baker, C. M.; Denning, E. J.; Nilsson, L.; MacKerell, A. D. Jr. J Chem Theory Comput 2012, 8, 348–362.
75. Cornell, W. D.; Cieplak, P.; Bayly, C. I.; Gould, I. R.; Merz, K. M.; Ferguson, D. M.; Spellmeyer, D. C.; Fox, T.; Caldwell, J. W.; Kollman, P. A. J Am Chem Soc 1995, 117, 5179–5197.
76. Perez, A.; Marchan, I.; Svozil, D.; Sponer, J.; Cheatham, T. E.; Laughton, C. A.; Orozco, M. Biophys J 2007, 92, 3817–3829.
77. Joung, I. S.; Cheatham, T. E. J Phys Chem B 2008, 112, 9020–9041.
78. van Dijk, M.; Bonvin, A. M. J. J Nucleic Acids Res 2009, 37, W235–W239.
79. Carson, S.; Wilson, J.; Aksimentiev, A.; Wanunu, M. Biophys J 2014, 107, 2381–2393.
80. Aksimentiev, A.; Heng, J. B.; Timp, G.; Schulten, K. Biophys J 2004, 87, 2086–2097.
81. Comer, J.; Dimitrov, V.; Zhao, Q.; Timp, G.; Aksimentiev, A. Biophys J 2009, 96, 593–608.
82. Wells, D. B.; Abramkina, V.; Aksimentiev, A. J Chem Phys 2007, 127, 125101.

Reviewing Editor: Nils Walter